Meteoritics & Planetary Science 41, Nr 10, 1437–1452 (2006)
Abstract available online at http://meteoritics.org

Ages of rampart craters in equatorial regions on Mars: Implications for the past and present distribution of ground ice

D. REISS[1*], S. VAN GASSELT[2], E. HAUBER[1], G. MICHAEL[1, 2], R. JAUMANN[1], and G. NEUKUM[2]

[1]Institute of Planetary Research, German Aerospace Center (DLR), Rutherfordstrasse 2, 12489 Berlin, Germany
[2]Institute for Geosciences, Freie Universitaet Berlin, Malteserstrasse 74-100, 12249 Berlin, Germany
[*]Corresponding author. E-mail: dennis.reiss@dlr.de

(Received 17 October 2005; revision accepted 09 May 2006)

Abstract–We are testing the idea of Squyres et al. (1992) that rampart craters on Mars may have formed over a significant time period and therefore the onset diameter (minimum diameter of a rampart crater) only reflects the ground ice depth at a given time. We measured crater size frequencies on the layered ejecta of rampart craters in three equatorial regions to derive absolute model ages and to constrain the regional volatile history. Nearly all rampart craters in the Xanthe Terra region are ~3.8 Gyr old. This corresponds to the Noachian fluvial activity that region. Rampart crater formation declines in the Hesperian, whereas onset diameters (minimum diameter) increase. No new rampart craters formed after the end of the Hesperian (~3 Gyr). This indicates a lowering of the ground ice table with time in the Xanthe Terra region. Most rampart craters in the Valles Marineris region are around 3.6 Gyr old. Only one large, probably Amazonian-aged (~2.5 Gyr), rampart crater exists. These ages indicate a volatile-rich period in the Early Hesperian and a lowering of the ground ice table with time in the Valles Marineris study region. Rampart craters in southern Chryse Planitia, which are partly eroded by fluvial activity, show ages around 3.9 Gyr. Rampart craters superposed on channels have ages between ~1.5 and ~0.6 Gyr. The onset diameter (3 km at ~1.5 Gyr) in this region may indicate a relatively shallow ground ice table. Loss of volatiles due to diffusion and sublimation might have lowered the ground ice table even in the southern Chryse Planitia region afterwards. In general, our study implies a formation of the smallest rampart craters within and/or shortly after periods of fluvial activity and a subsequent lowering of the ground ice table indicated by increasing onset diameter to the present. These results question the method to derive present equatorial ground ice depths from the onset diameter of rampart craters without information about their formation time.

INTRODUCTION

Many large craters on Mars are surrounded by fluidized or lobate ejecta morphologies (Head and Roth 1976; Carr et al. 1977; Mouginis-Mark 1979), which are not observed on other terrestrial planets like the Moon or Mercury. The morphology of these rampart craters is suggested to be caused by the impact process in volatile rich target material (e.g., Carr et al. 1977; Wohletz and Sheridan 1983; Mouginis-Mark 1987) or atmospheric effects (Schultz and Gault 1979; Schultz 1992; Barnouin-Jha and Schultz 1998; Barnouin-Jha et al. 1999a, 1999b; for a summary and discussion about the two formation theories see review by Barlow 2005). Although most researchers favor the idea that subsurface volatiles cause the fluidized ejecta morphologies on Mars, we will use in the following the standardized term "layered morphology" of the Mars Crater Morphology Consortium (Barlow et al. 2000) for describing the ejecta or the term "rampart crater" in general to avoid references to the possible origins of these features. Previous studies showed that rampart craters occur in all geological units and at all altitudes and latitudes (Allen 1979; Mouginis-Mark 1979; Kuzmin et al. 1988; Costard 1989; Barlow and Bradley 1990). However, there exist correlations of diameter with latitude. In a given area, a certain minimum diameter exists for rampart craters, called the onset diameter (Boyce and Witbeck 1980; Kuzmin 1980). Geographic mapping shows a latitude dependence of the onset diameters (Mouginis-Mark 1979; Kuzmin et al. 1988; Costard 1989). In equatorial regions they are typically 4 to 7 km versus 1 to 2 km at high latitudes (50° latitude) (Squyres et al. 1992), which might indicate an ice rich layer at depths of ~300 m to ~400 m near the equator and ~100 m at 50° latitude (Kuzmin

et al. 1989). However, more recent work has shown that the equatorial onset diameter varies regionally (Barlow et al. 2001) and can be as small as 1 km (Reiss et al. 2005), equal to those at high latitudes.

As pointed out by, e.g., Squyres et al. (1992), rampart craters may have formed over a significant time interval and therefore the onset diameter reflects the ground ice depth at a given time. The time of the impact events and, therefore, the absolute age of the layered ejecta morphologies is unknown. Barlow (2004) compared an ejecta mobility (EM) ratio with a preservation classification system of rampart craters in different geologic units within the equatorial zone. This relative age determination study indicates that the concentrations of subsurface volatiles remained approximately constant with respect to depth and time (Barlow 2004). Based on its morphology Mouginis-Mark et al. (2003) attributed a very young age to a large (~29 km) rampart crater west of Olympus Mons, which may indicate that volatiles still exist within the top kilometers of the near equatorial region of Mars.

We determined the absolute model ages of rampart craters in three equatorial regions on Mars by measuring the layered ejecta superposed crater size frequencies in Mars Express High-Resolution Stereo Camera (HRSC) imagery (Neukum et al. 2004b). The images used for our measurements have a resolution between 12 and 15 m/pxl and cover large areas (~10^5 km^2), which allows us to determine small crater diameters and to work in a regional context. The derived ages of the rampart craters in combination with a regional onset diameter at a given time give us an estimate of the volatile history in the study regions.

METHODOLOGY

To determine the absolute model ages of the rampart craters, we measured the crater size frequencies on the ejecta blankets using the Martian impact cratering model of Hartmann and Neukum (2001) and the coefficients of Ivanov (2001). Absolute age determinations for Mars are obtained from the lunar crater production curve using Martian crater scaling laws (Soderblom et al. 1974; Neukum and Wise 1976; Neukum and Hiller 1981; Stöffler and Ryder 2001; Hartmann 1977; Ivanov 2001; Neukum et al. 2001). The ages from crater counts are limited in accuracy by the statistical error (Neukum et al. 2001). Other error sources, such as undetected admixtures of secondary craters are normally minor (<10% of the frequency of superposed craters) (Neukum et al. 2001; Hartmann and Neukum 2001). The statistical errors of individual data points are mostly <30% (one standard deviation, 1σ). Because the whole distribution over a wider crater size range is used for fitting the theoretical size-frequency distribution to the measurements, the average statistical error of the data points over the ensemble of measurement is the proper measure for the uncertainty, resulting in an average uncertainty of 20–30% in frequency (Neukum et al. 2004a). This translates into a 20–30% uncertainty in the absolute ages for ages younger than 3 Gyr and an uncertainty of only 100–200 Myr for ages older than 3 Gyr (Neukum et al. 2004a). Absolute ages of young surfaces (<2 Gyr) may be affected by a possible systematic error of about a factor of two in the crater frequency, primarily arising from the uncertainty in the Mars/Moon cratering rate ratio (Hartmann and Neukum 2001; Ivanov 2001).

We are aware that absolute age determinations using the techniques described above are currently debated because of the secondary crater issue (McEwen et al. 2005; Hartmann 2005), which might affect the cratering chronology of crater diameters smaller than approximately 500 m (McEwen et al. 2005). Recent studies of Werner et al. (2006) showed that the steep branch of size-frequencies distributions is not dominated by secondaries and that the secondary crater contribution is less than 10%. In this context, it is worth mentioning that all geologic units on which crater counts have been performed were carefully mapped. Cluster fields indicating secondary cratering have been excluded from the mapping and therefore the counting process. However, the derived absolute model ages from this study are mostly based on crater diameters between ~600 m and more than one kilometer. Only three of 71 (4%) age determinations of rampart craters are based on crater diameters smaller than 500 m due to the lack of larger craters on the layered ejecta blankets. This and the differences of ages in different areas suggest that secondary cratering is not contributing significantly to our results and lead us to have confidence in these results.

To give some estimates about the maximum depths of the possible ground ice table, we derived the excavation depths (d_e) using the depth-diameter relationship method described in Barlow (2005):

$$D_t = D_{sc}^{0.15 \pm 0.04} D_r^{0.85 \pm 0.04} \quad (1)$$

For complex craters (>7 km), the transient diameter (D_t) of the crater is estimated from the current crater rim diameter (D_r) (Croft 1985), where D_{sc} is the simple to complex transition, which is ~7 km for Martian impact craters (Garvin et al. 2000). For simple craters (<7 km), the transient diameter (D_t) is approximately equal to the observed crater rim diameter. The excavation depth (d_e) is then derived assuming $d_e \approx D_t/10$ (Melosh 1989).

STUDY REGIONS

The study regions are located in the Xanthe Terra region between Maja Vallis to the west and Shalbatana Vallis to the east (0–15°N and 310–314°E), in the Valles Marineris region across the Tithonium and Ius Chasmata to the eastern part of Sinai Planum (17°S–6°N and 276.5–281°E) and in southern Chryse Planitia west of the Pathfinder landing site

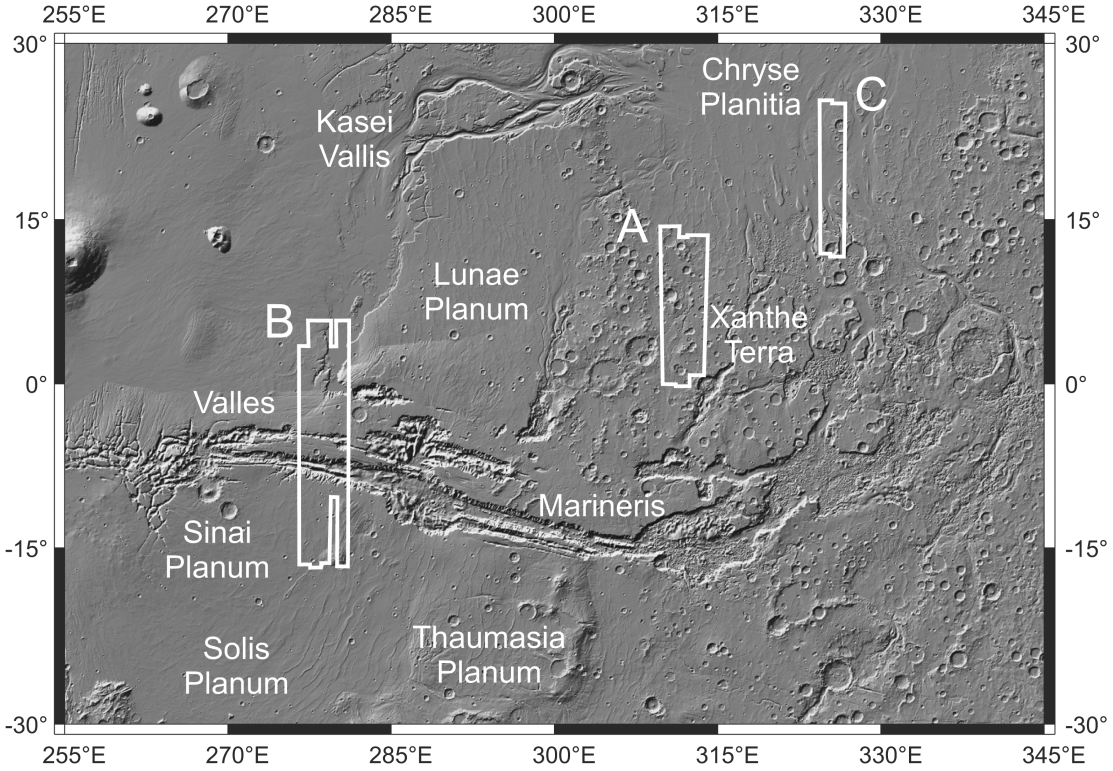

Fig. 1. The regional context of the study areas. White frames show the locations of image mosaics in Figs. 2, 5, and 9. a) An HRSC-image mosaic of orbits 927, 905, and 894 in the Xanthe Terra region. b) An HRSC-image mosaic of orbits 1143 and 1154 in southern Chryse Planitia. c) An HRSC-image mosaic of orbits 71, 97, 887, 920, and 931 in the Valles Marineris region.

(11.8–25.6°N and 324.5–326.7°E) (Fig. 1). These regions were selected because of their main location in three different geologic epochs (Noachian, Hesperian, and Amazonian). Furthermore, in all three regions, different fluvial processes such as groundwater sapping, surface runoff, and catastrophic floods were active during these geologic epochs, which indicate volatile-rich periods. In the following chapters, we will describe the results and discuss the implications for these regions individually.

Xanthe Terra

Geological Context

The study area of Xanthe Terra is located south of Chryse Planitia and north of Valles Marineris (Fig. 2). The region lies mostly in the Noachian-aged subdued cratered unit (Npl_2) (Scott and Tanaka 1986). Several valley networks (Nanedi, Hyphanis, and Sabrina Vallis) cut the region. Two larger areas in the southwestern and midwestern part belong to the cratered unit (Npl_1), and small areas in the northern part belong to the hilly unit (Nplh) (Scott and Tanaka 1986). The northeastern part of the study region is located at the transition of the heavily cratered highlands into the northern lowlands (Chryse basin), which consists of Hesperian-aged ridged plains material (Hr) (Scott and Tanaka 1986).

Results

Ages of rampart craters in the Xanthe Terra region (Figs. 3 and 4; Table 1) are in the range of ~4 to ~3 Gyr. Most absolute model ages of individual ejecta blankets are around 3.8 Gyr. The youngest measured ages of rampart craters (~3.0 Gyr and ~3.2 Gyr) are located on Hesperian units in the northeast of the study region (Figs. 2 and 4b). The formation rate of rampart craters declines in the Hesperian, whereas the onset diameter increases (Fig. 3). At the Hesperian-Amazonian boundary, the formation comes to an end. Several rampart craters show relative age relationships to fluvial features (Fig. 4a). Some rampart craters are superposed on valley networks and some fluvial features are eroded into the layered ejecta morphology. The ages of these rampart craters are between ~3.5 and ~4.0 Gyr.

Implications

Several relative age relationships between rampart craters and fluvial features by superposition of rampart craters upon valley networks as well as fluvial eroded layered ejecta by lateral valleys indicate that the formation of rampart craters and fluvial erosion are strongly connected in this region. The derived ages (~3.8 Gyr) imply that their formation is connected with the Late Noachian fluvial activity in this region (Masursky et al. 1977, 1980).

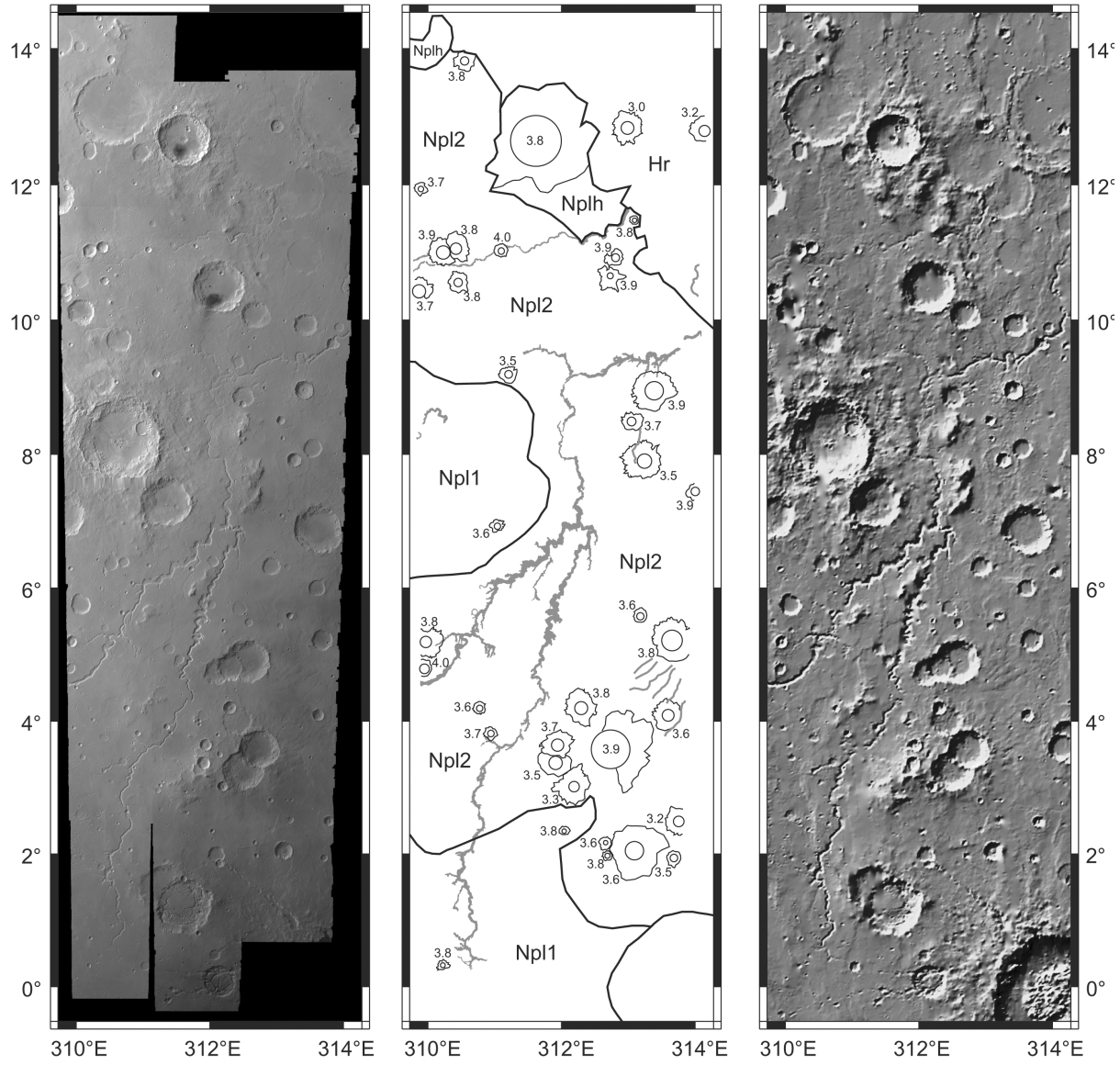

Fig. 2. An HRSC-image mosaic of orbits 927, 905, and 894 (left); a map of rampart craters with ages and major geologic units (middle); and a shaded relief from Mars Orbiter Laser Altimeter (MOLA) data (right) in the Xanthe Terra region from 309.75–314.25°E and 0.5°S–14.5°N. Absolute model ages of rampart craters are shown by numbers near the mapped ejecta blankets. Main geological units (modified after Scott and Tanaka 1986) are separated by black lines. Fluvial features are shown in gray color.

It is obvious that most rampart craters (75%) are located on the subdued cratered unit (Npl_2–Late Noachian) (Fig. 2), the age of which (~3.8 Gyr) is approximately consistent with most of the determined ages of the rampart craters. It is likely that the formation of rampart craters began shortly after the formation of this unit. The high frequency of rampart craters and dissection by valley networks of this unit (Npl_2) in contrast to the older cratered unit (Npl_1) might indicate a favorable region for groundwater that led to the formation of valley networks and rampart craters.

The lack of Amazonian-aged rampart craters and increasing onset diameter from the Noachian to late Hesperian indicate a lowering of the ground ice table with time, which in Xanthe Terra, if present at all, could be several kilometers deep at the present time. The estimated depth of the ground ice table derived from the excavation depth (d_e) of the onset diameter at a given time suggests a decrease from ~400 m in the Noachian to ~1 km at the Hesperian-Amazonian boundary. Either all ground ice was lost with time due to diffusion to the atmosphere (e.g., Carr 1996) or there is still a deep ground ice layer that can only be reached by relatively large (and in recent times rare) impacts.

Inner channels in Nanedi Vallis (Carr and Malin 2000) and paleolacustrine deposits in Xanthe Terra (Hauber et al. 2005; Di Achille et al. 2006) indicate sustained flow and

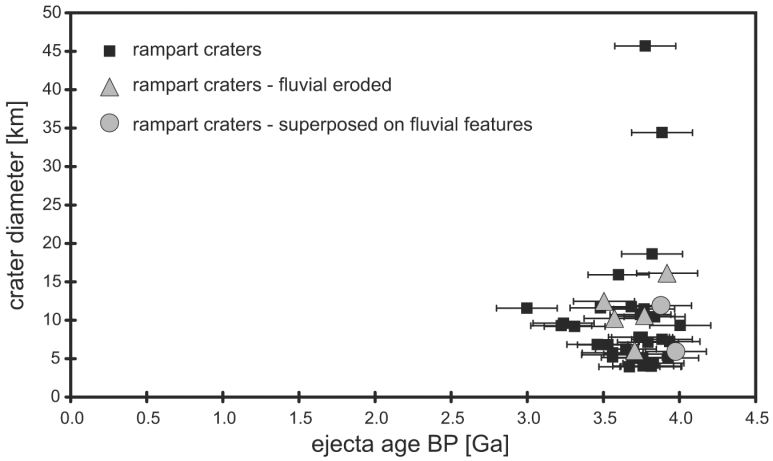

Fig. 3. Absolute model ages of rampart craters versus crater diameter of the Xanthe Terra region. Gray triangles show ejecta blankets that are superposed on fluvial features. Gray circles show ejecta blankets that are eroded by fluvial activity. Black squares show no relative age relationships. Error bars are 30% for absolute model ages younger than 3 Gyr and ±200 Myr for absolute model ages ≥3 Gyr (Neukum et al. 2004a).

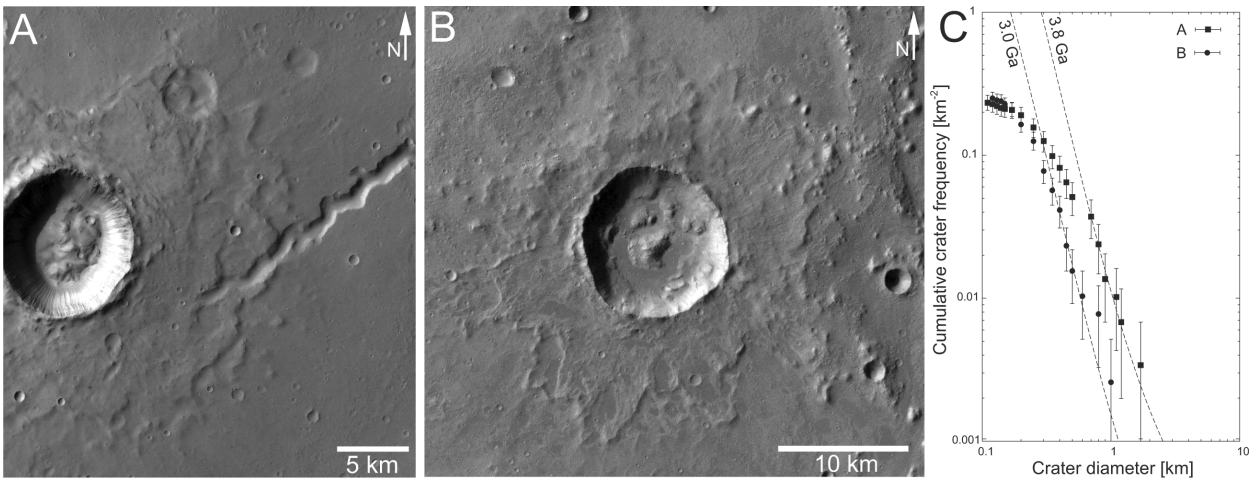

Fig. 4. Rampart craters in the Xanthe Terra region. a) A lateral valley of Nanedi Vallis eroded into the ejecta blanket with an absolute model age of ~3.8 Gyr (HRSC-orbit 927 at 5.2°N and 310°E, D = 10.5 km). b) The youngest measured ejecta blanket in this study region with an absolute model age of ~3.0 Gyr, located in the southwest part of Chyrse Planitia (HRSC-orbit 894 at 12.84°N and 313°E, D = 11.6 km). c) Crater size-frequency data and derived absolute ages of A and B. Error bars: 1σ error.

standing bodies of water. Valley formation might have begun in the Noachian and continued into the Early Hesperian (Masursky et al. 1977, 1980; Rotto and Tanaka 1995; Crumpler 1997). Carr and Malin (2000) suggest downstream erosion instead of sapping related headward erosion for the main channel of Nanedi Vallis, but they conclude that the tributaries of the main valley may have formed by sapping. Our results may support this view. The smallest rampart craters occur at around 3.8 Gyr, which might indicate that surface water may have been present in the Late Noachian. The increasing onset diameter into the Hesperian may be consistent with a transition of surface water processes to groundwater related processes such as sapping. However, it is worth noting that we did not find very small rampart craters ≤1 km in the Xanthe Terra region, which would indicate near-surface volatiles.

Valles Marineris

Geological Context

The study region is a long and narrow, north–south oriented traverse from south of Echus Chasma, across the Tithonium and Ius Chasmata to the eastern part of Sinai Planum (17°S–6°N and 276.5°–281°E) (Fig. 5). Most of the plateau units are of Hesperian age (Fig. 5) (Scott and Tanaka 1986). Only small regions like the interior of Echus Chasma in the north and the Valles Marineris interior deposits consist of Amazonian-aged materials. In the southeast there are small

Table 1. The size, location, absolute model age, crater retention age, and geological unit of observed rampart craters in the Xanthe Terra region.

Diameter (km)	Longitude (°E)	Latitude (°)	Age (Gyr)	N(1)[a]	Geological unit[b]
3.93	313.1	11.48	3.8	1.12E-02	Npl_2
3.95	312.67	2.18	3.7	5.39E-03	Npl_2
4.01	310.21	0.34	3.8	1.16E-02	Npl_1
4.04	312.04	2.36	3.8	8.59E-03	Npl_2
4.41	312.69	1.99	3.8	1.26E-02	Npl_2
5.08	312.73	10.66	3.9	2.28E-02	Npl_2
5.1	312.73	10.66	3.8	8.47E-03	Npl_2
5.15	309.88	11.95	3.7	5.82E-03	Npl_2
5.5	311.03	6.94	3.6	3.37E-03	Npl_1
5.6	310.93	3.83	3.7	6.28E-03	Npl_2
5.76	310.76	4.2	3.6	3.41E-03	Npl_2
5.93	311.09	11.03	4	3.17E-02	Npl_2
6.23	313.18	5.6	3.6	4.85E-03	Npl_2
6.81	313.69	1.96	3.5	3.07E-03	Npl_2
6.84	311.2	9.2	3.5	2.53E-03	Npl_2
7.13	310.54	13.82	3.8	1.02E-02	Npl_2
7.23	312.81	10.94	3.9	2.43E-02	Npl_2
7.51	314	7.45	3.9	1.77E-02	Npl_2
7.78	310.44	10.56	3.8	8.25E-03	Npl_2
7.8	313.05	8.49	3.7	7.37E-03	Npl_2
9.18	312.19	3.03	3.3	1.91E-03	Npl_2
9.3	313.76	2.5	3.2	1.73E-03	Npl_2
9.32	309.93	4.8	4	3.84E-02	Npl_2
9.61	314.14	12.8	3.2	1.76E-03	Hr
10.24	313.61	4.1	3.6	3.57E-03	Npl_2
10.46	310.4	11.07	3.8	1.32E-02	Npl_2
10.52	309.95	5.2	3.8	9.01E-03	Npl_2
10.74	311.94	3.64	3.7	7.76E-03	Npl_2
11.45	312.29	4.21	3.8	8.86E-03	Npl_2
11.58	312.99	12.84	3	1.49E-03	Hr
11.61	311.91	3.39	3.5	2.66E-03	Npl_2
11.76	309.85	10.43	3.7	5.72E-03	Npl_2
11.9	310.22	11.01	3.9	1.71E-02	Npl_2
12.45	313.25	7.92	3.5	2.84E-03	Npl_2
15.92	313.09	2.06	3.6	3.95E-03	Npl_2
16.12	313.39	8.96	3.9	2.19E-02	Npl_2
18.62	313.66	5.22	3.8	1.19E-02	Npl_2
34.42	312.72	3.59	3.9	1.78E-02	Npl_2
45.69	311.61	12.67	3.8	9.25E-03	Nplh

[a]N(1) is the cumulative number of craters with diameters equal to or larger than 1 km per square kilometer. The N(1) values have been derived by measurements. Smaller crater sizes have been recalculated for sizes of 1 km through application of the Neukum crater SFD.
[b]After Scott and Tanaka (1986).

Noachian-aged units. The Hesperian units Hr, Hsu, Hpl_3, and Hf consist mainly of lava flows; some are covered by dust deposits (Scott and Tanaka 1986).

Results

Most rampart craters in the Valles Marineris region show absolute model ages between ~3.9 Gyr and ~3.0 Gyr (Figs. 6 and 7; Table 2). One rampart crater shows an absolute model age of ~2.5 Gyr (Fig. 7b). It is noteworthy that the layered ejecta cover the ejecta blankets of two other rampart craters with derived model ages of ~3.5 Gyr and ~3.6 Gyr (Fig. 5). The relative as well as absolute ages are in agreement. Furthermore, the layered ejecta have a morphologically fresh appearance and the crater itself is bowl-shaped with sharp rims, which indicates low degradation since its formation. The smallest craters with measurable age layered ejecta blankets are around 3.6 Gyr old. However, a large number (20) of unusually small equatorial rampart craters with diameters from 1 km to 4 km exist in this region (Reiss et al. 2005) (Fig. 8; Table 2). Crater counts on their layered ejecta blankets are not possible due to their small areal extent and high degradation.

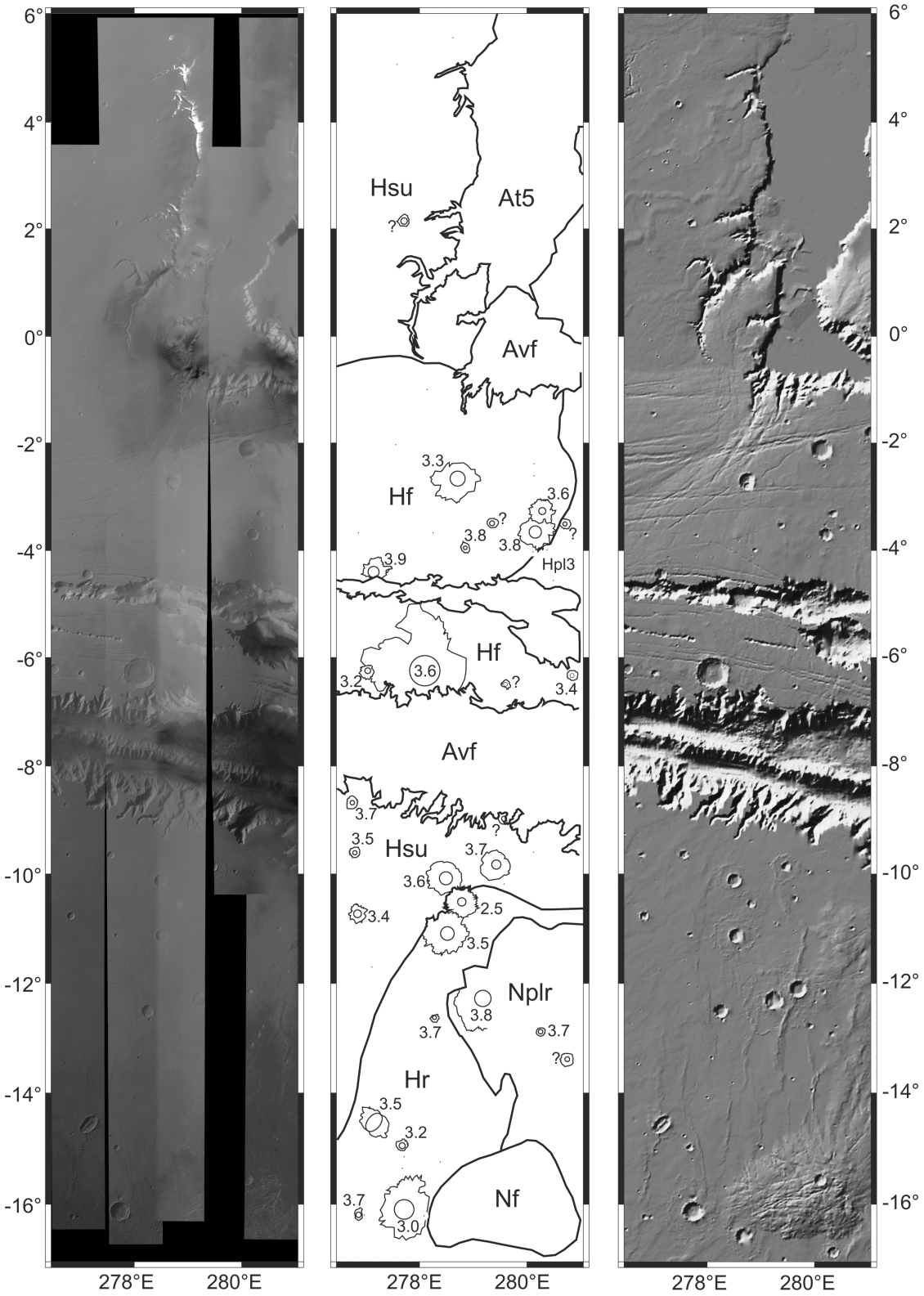

Fig. 5. An HRSC-image mosaic of orbits 71, 97, 887, 920, and 931 (left); a map of rampart craters with ages and major geologic units (middle); and a shaded relief from Mars Orbiter Laser Altimeter (MOLA) data (right) in the Valles Marineris region from 276.5–281°E and 17°S–6°N. Absolute model ages of rampart craters are shown by numbers near the mapped ejecta blankets. Main geological units (modified after Scott and Tanaka 1986) are separated by black lines. Rampart craters smaller than 4 km are shown as black circles.

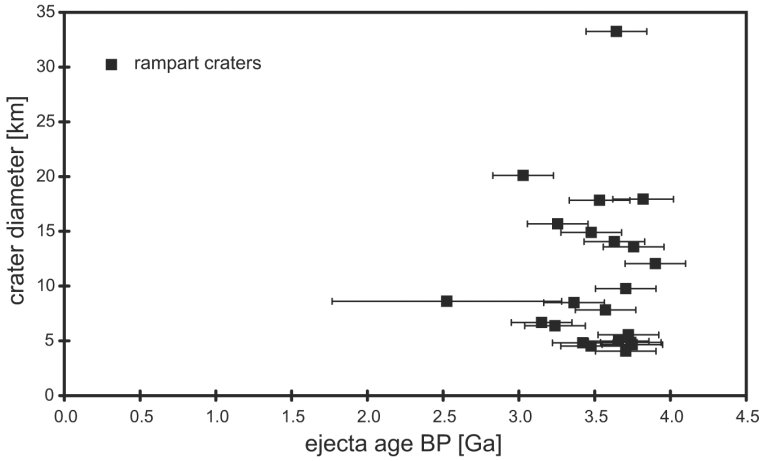

Fig. 6. Absolute model ages of rampart craters versus crater diameter of the Valles Marineris region. Error bars are 30% for absolute model ages younger than 3 Gyr and ±200 Myr for absolute model ages ≥3 Gyr (Neukum et al. 2004a).

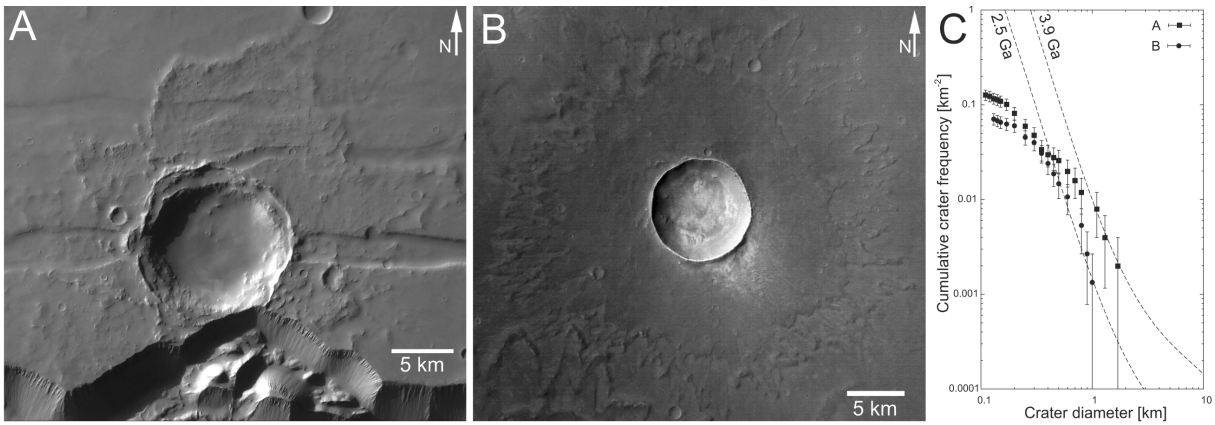

Fig. 7. Rampart craters in the Vallis Marineris region. a) An example of an old rampart crater with an absolute model age of ~3.9 Gyr. The ejecta blanket is eroded by Tithonium Chasma and smaller grabens (HRSC-orbit 931 at 4.49°S and 277.17°E, D = 12.3 km). b) An example of a young rampart crater with an absolute model age of ~2.5 Gyr. The ejecta blanket superposes two older ejecta blankets in the northwest and southwest (HRSC-orbit 97 at 10.65°S and 278.82°E, D = 8.6 km). c) Crater size-frequency data and derived absolute ages of (a) and (b). Error bars: 1σ error.

Implications

The small rampart craters with an onset diameter of 1 km indicate near surface ice at the time of the impacts in this region. The degraded ejecta blankets as well as the lower depth-diameter ratios of the rampart craters in contrast to pristine craters of the same region indicate old, most likely Hesperian ages (Reiss et al. 2005). The smallest rampart craters for which we were able to determine absolute model ages in this study are around 3.6 Gyr old. It seems plausible, although it can not be proved, that the smaller rampart craters (where age determinations are not possible) were also formed around 3.6 Gyr ago. This would explain the lower depth/diameter ratios in contrast to pristine craters due to erosional and depositional processes and the highly degraded layered ejecta morphologies (Reiss et al. 2005).

Small onset diameters and ages of rampart craters in the Valles Marineris region indicate a shallow ground ice table (~100 m) in the Hesperian. The lack of smaller rampart craters in the Amazonian and the increasing onset diameter after around 3.6 Gyr indicate a lowering of the ground ice table. The present ground ice table in this region might be several hundred meters (~800 m) deep, as indicated by a relatively large (D = 8.61 km) Amazonian-aged rampart crater. However, this rampart crater, which formed approximately 2.5 Gyr ago, is still very old and the possible ongoing diffusion/sublimation of ground ice might have further lowered the ground ice table in this region.

This scenario would be in agreement with the observed volatile history of Valles Marineris. Several surface features suggest the presence of liquid water in the Valles Marineris region: the detection of sulfates, which might have formed as evaporites (Gendrin et al. 2005), sapping valleys formed by groundwater seepage and subsequent backward erosion (Higgins 1982), spur-and-gully morphology might have also

Table 2. The size, location, absolute model age, crater retention age, and geological unit of observed rampart craters in the Valles Marineris region.

Diameter (km)	Longitude (°E)	Latitude (°)	Age (Gyr)	N(1)[a]	Geological unit[b]
1.08	278.29	–3.75	n.d.	n.d.	Hf
1.41	278.42	–15.44	n.d.	n.d.	Hr
1.56	277.71	–15.55	n.d.	n.d.	Hr
1.57	279.6	–10.32	n.d.	n.d.	Hsu
1.76	277.15	–11.86	n.d.	n.d.	Hsu
1.79	276.79	–9.84	n.d.	n.d.	Hsu
1.86	280.14	–9.73	n.d.	n.d.	Hsu
1.91	280.16	–2.67	n.d.	n.d.	Hf
1.91	277.75	–15.34	n.d.	n.d.	Hr
2.29	278.12	–16.42	n.d.	n.d.	Hr
2.31	280.39	–4.07	n.d.	n.d.	Hpl_3
2.53	280.15	–2.44	n.d.	n.d.	Hf
2.64	277.59	–2.09	n.d.	n.d.	Hf
2.73	277.62	5.09	n.d.	n.d.	Hsu
2.97	280.51	–4.64	n.d.	n.d.	Hpl_3
3	278.66	5.59	n.d.	n.d.	Hsu
3.22	276.91	–3.75	n.d.	n.d.	Hf
3.36	280.13	–4.11	n.d.	n.d.	Hf
3.48	278.18	–1.04	n.d.	n.d.	Hf
3.51	276.99	–16.38	n.d.	n.d.	Hr
4.06	278.3	–12.79	3.7	6.37E-03	Hr
4.41	279.62	–6.6	n.d.	n.d.	Hf
4.49	280.74	–3.59	n.d.	n.d.	Hpl_3
4.54	276.81	–9.74	3.5	2.63E-03	Hsu
4.67	278.88	–4.03	3.7	7.99E-03	Hpl_3
4.82	280.87	–6.44	3.4	2.30E-03	Hf
4.86	276.77	–8.81	3.7	7.58E-03	Hsu
4.98	280.28	–13.05	3.7	5.08E-03	Nplr
5.01	280.78	–13.55	n.d.	n.d.	Nplr
5.33	279.59	–9.11	n.d.	n.d.	Hsu
5.56	276.88	–16.88	3.7	6.96E-03	Hr
6.38	277.06	–6.35	3.2	1.76E-03	Hf
6.68	277.7	–15.13	3.1	1.63E-03	Hr
7.83	280.31	–3.35	3.6	3.55E-03	Hpl_3
8.49	276.87	–10.87	3.4	2.07E-03	Hsu
8.61	278.82	–10.65	2.5	1.23E-03	Hr
9.76	279.45	–9.95	3.7	6.37E-03	Hsu
12.3	277.17	–4.49	3.9	1.11E-02	Hf
13.58	280.18	–3.74	3.8	8.37E-03	Hpl_3
14.07	278.51	–10.51	3.6	4.48E-03	Hsu
14.9	278.54	–11.23	3.5	2.64E-03	Hr
15.68	278.74	–2.72	3.3	1.79E-03	Hf
17.83	277.21	–14.69	3.5	3.10E-03	Hr
17.94	279.23	–12.42	3.8	1.20E-02	Nplr
20.1	277.76	–16.28	3	1.52E-03	Hr
33.25	278.11	–6.35	3.6	4.76E-03	Hf

[a]N(1) is the cumulative number of craters with diameters equal to or larger than 1 km per square kilometer. The N(1) values have been derived by measurements. Smaller crater sizes have been recalculated for sizes of 1 km through application of the Neukum crater SFD.
[b]After Scott and Tanaka (1986).

formed by the action of liquid water (Jernsletten 2004), and the morphologies and ages of landslides seem to indicate that liquid water might have been present in the walls during their erosion (Lucchitta 1987; Quantin et al. 2004).

It seems plausible that an initially shallow groundwater table existed simultaneously with the Hesperian-aged fluvial activity in the same area (Mangold et al. 2004; Harrison and Grimm 2005), and was subsequently lowered by the formation of the Valles Marineris due to sapping into the basin and trough interiors, where the water might have

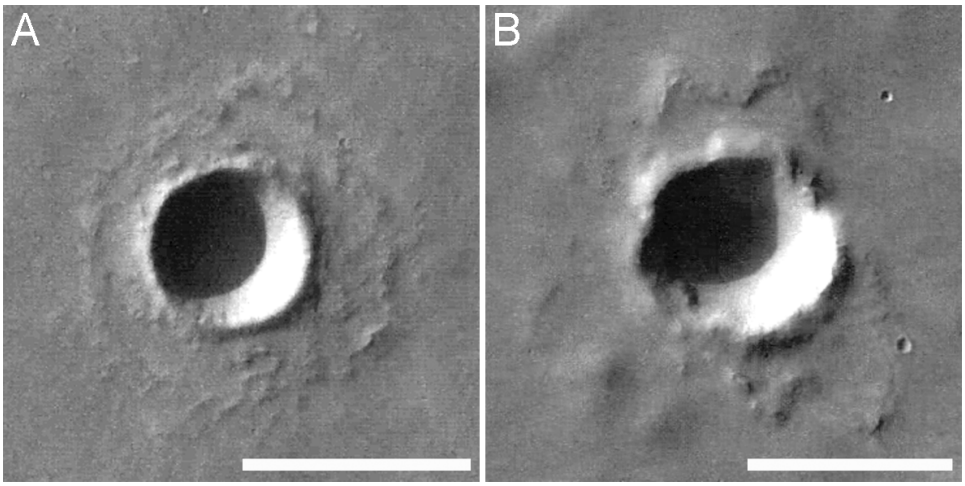

Fig. 8. Examples of small rampart craters. Scale bars for all images are 2 km; north is at the top. a) HRSC-orbit 920 at 15.44°S and 278.42°E; D = 1.41 km. b) HRSC-orbit 887 at 9.73°S and 280.14°E; D = 1.86 km.

ponded and finally evaporated. This scenario would also be in agreement with a slow transition from wet to dry conditions in Valles Marineris (Peulvast et al. 2001).

Our results indicate a shallow ground ice table in the Early Hesperian (around 3.6 Gyr). Therefore, we favor an Early Hesperian age for the dendritic valley networks near Echus Chasma as Harrison and Grimm (2005) suggest in contrast to Mangold et al. (2004) and Quantin et al. (2005) who derived a Late Hesperian age.

Chryse Planitia

Geological Context

The study area of southern Chryse Planitia (west of the Pathfinder landing site) covers the northern part of the outflow channels Tiu Vallis and the northwestern part of Ares Vallis (Fig. 9). The southern area of this study region consists geologically of Noachian-aged highland material (Npl_1) (Scott and Tanaka 1986), which is dissected by Tiu and Ares Vallis. Several streamlined islands are also remnants of the southern highlands (Npl_1). The channel floors in the south are covered by channel deposits (Hch) and most parts of the northern study area are covered by flood-plain material (Hchp) (Scott and Tanaka 1986). One region in the northern area belongs to the northern plains assemblage (Aa_4) (Scott and Tanaka 1986), which partly buried the flood-plain material (Hchp). This unit type is interpreted as lava flows, which emerged from small volcanoes (Scott and Tanaka 1986).

Results

In southern Chryse Planitia, the rampart craters with ejecta eroded by fluvial events show absolute model ages around 3.8 Gyr and between ~1.5 and ~0.6 Gyr for channel superposed rampart craters (Figs. 10 and 11; Table 3). For one rampart crater (Yuty at 325.9°E and 22.4°N, D = 19.2 km), it is unclear whether the last fluvial event was able to erode its ejecta. Yuty is located on flood-plain material (Hchp); the ejecta blanket shows no signs of fluvial erosion and has an absolute model age of ~2.2 Gyr. It is possible that the youngest fluvial activity was flows in the confined channels (Hch) that did not affect the topographically higher floodplain units (Hchp).

Implications

Most investigators favored a catastrophic-flood origin of the Mars Pathfinder landing site (e.g., Golombek et al. 1997; Komatsu and Baker 1997); others suggested an origin by ice flow (Lucchitta 1998) or debris flows (Tanaka 1999). The main activity phase of the circum-Chryse outflow channels is suggested between ~3.8 and ~3.0 Gyr, but might have lasted with lower activity into the Amazonian (Masursky et al. 1977; Baker and Kochel 1979; Carr and Clow 1981). Based on morphologic and stratigraphic superposition relationships of the circum-Chryse outflow channels, Tiu Vallis shows the youngest relative age (Tanaka 1997; Nelson and Greeley 1999; Ivanov and Head 2001). Absolute model age determinations of channel floors revealed that the fluvial activity of Tiu Vallis occurred in the range between ~3.6 to ~1.5 Gyr B.P. (Neukum and Hiller 1981; Marchenko et al. 1998). These age determinations are in good agreement with the ages of rampart craters in the study region and confirm the measured channel floor ages of Neukum and Hiller (1981) and Marchenko et al. (1998).

The formation of one young Amazonian-aged rampart crater with a diameter of ~3 km indicates that ground ice could still be present in this region at depths of a few hundred meters (~300 m). The ground ice might have been recharged by the last fluvial episode of Tiu Vallis and sheltered from diffusion by thick fluvial sediments or subsequent lava flows. However, this small rampart crater has an absolute model age of around ~1.5 Gyr and seems to have been formed shortly after the last fluvial event, where subsurface volatiles were

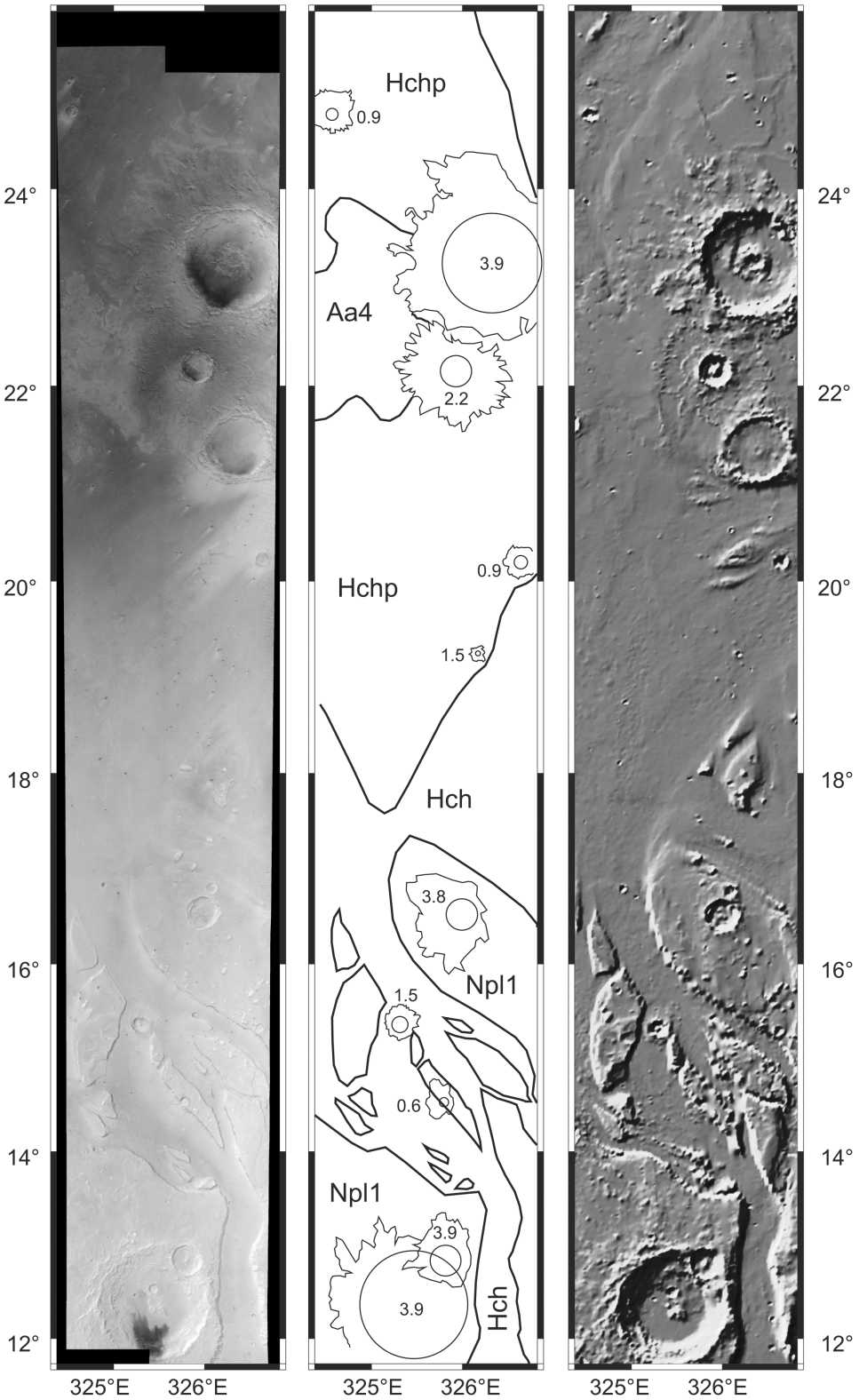

Fig. 9. An HRSC-image mosaic of orbits 1143 and 1154 (left); a map of rampart craters with ages and major geologic units (middle); and a shaded relief from Mars Orbiter Laser Altimeter (MOLA) data (right) of southern Chryse Planitia from 324.4–326.8°E and 11.75–25.75°N. Absolute model ages of rampart craters are shown by numbers near the mapped ejecta blankets. Main geological units (modified after Scott and Tanaka 1986) are separated by black lines.

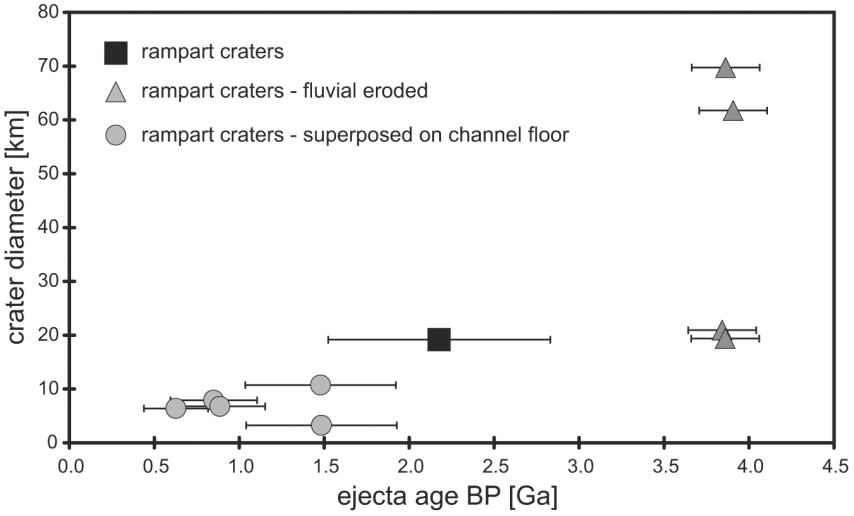

Fig. 10. Absolute model ages of rampart craters versus crater diameter of southern Chryse Planitia. Gray triangles show ejecta blankets that are superposed on the channel floors. Gray circles show ejecta blankets that are eroded by fluvial activity. Black squares show no relative age relationships. Error bars are 30% for absolute model ages younger than 3 Gyr and ±200 Myr for absolute model ages ≥3 Gyr (Neukum et al. 2004a).

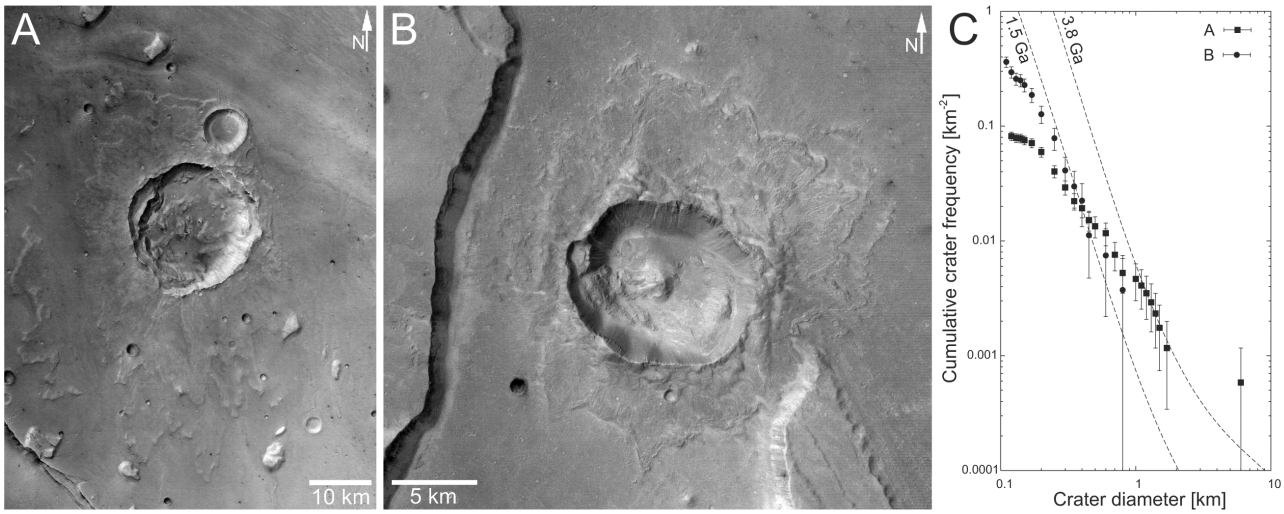

Fig. 11. Rampart craters in southern Chryse Planitia. a) An example of an old rampart crater with an absolute model age of ~3.8 Gyr. The ejecta blanket is eroded by fluvial activity of Ares and Tiu Vallis (HRSC-orbit 1154 at 15.51°N and 325.3°E, D = 20.2 km). b) An example of a young rampart crater with an absolute model age of ~1.5 Gyr, which superposes the channel floor of Tiu Vallis (HRSC-orbit 1143 at 16.71°N and 326°E, D = 10.75 km). c) Crater size-frequency data and derived absolute ages of (a) and (b). Error bars: 1σ error.

likely present. Three younger, larger rampart craters formed on the channel floors, suggesting that ground-ice depths between ~600 m and ~800 m might indicate that ground ice was lost over time in the Amazonian, because smaller craters are formed statistically more frequently. A shallow ground ice table after the last catastrophic fluvial recharge might be not sufficiently stable to remain for longer times.

DISCUSSION

The results of this study suggest that the formation of rampart craters is connected with regional volatile-rich periods in Martian history. The measurable model ages of craters with the smallest diameters are within the range of times when fluvial processes were active or shortly after. After these volatile-rich periods, there is a trend that only larger craters exhibit the layered ejecta morphology. The onset diameter increases with time, which might indicate a general lowering of the ground ice table in the Xanthe Terra and Valles Marineris study regions throughout geologic history. A lowering of the ground ice table possibly occurred also after the last groundwater recharge in southern Chryse Planitia. This would be consistent with a loss of ground ice in equatorial regions throughout geologic history (Clifford and

Table 3. The size, location, absolute model age, crater retention age, and geological unit of observed rampart craters in southern Chryse Planitia.

Diameter (km)	Longitude (°E)	Latitude (°)	Age (Gyr)	N(1)[a]	Geological unit[b]
3.01	326.16	19.46	1.5	7.23E-04	Hchp
6.38	325.79	14.69	0.6	3.06E-04	Hch/Npl_1
6.75	324.56	24.98	0.9	4.32E-04	Hchp
7.9	326.62	20.42	0.8	4.14E-04	Hchp
10.74	325.3	15.51	1.5	7.21E-04	Hch
19.15	325.91	22.39	2.2	1.06E-03	Hchp
19.37	325.81	12.98	3.9	1.52E-02	Npl_1
20.23	325.99	16.71	3.8	1.36E-02	Npl_1
61.76	326.31	23.48	3.9	2.03E-02	Hchp
69.75	325.44	12.52	3.9	1.54E-02	Npl_1

[a]N(1) is the cumulative number of craters with diameters equal to or larger than 1 km per square kilometer. The N(1) values have been derived by measurements. Smaller crater sizes have been recalculated for sizes of 1 km through application of the Neukum crater SFD.
[b]After Scott and Tanaka (1986).

Hillel 1983; Fanale et al. 1986; Clifford 1993) rather than the persistence of ground ice at shallow depths (Mellon and Jakosky 1995; Mellon et al. 1997) in the study regions.

The analysis of Barlow (2004) revealed that concentrations of subsurface volatiles have remained approximately constant at the depths and over the time periods recorded by the investigated equatorial rampart craters. This study is based on relative crater depth, rim sharpness, ejecta blanket preservation, interior feature preservation, and the thermal inertia of larger rampart craters (Barlow 2004). The resulting preservation class was then compared with the ejecta mobility (EM), which might indicate changes in the subsurface volatile concentrations. The results of Barlow (2004) imply no major variation in subsurface ice concentration with time at greater depths (generally >1 km due to the investigated large rampart craters). Our regional studies based on the onset diameter generally indicates a loss of volatiles in the shallow subsurface with time and possible present-day ground ice table depths at ~1 km. These results are not in contrast, but the study of Barlow (2004) is limited to greater depths, while our study is regionally limited. However, additional studies using both methods may further constrain changes in the subsurface ice concentration and depth with time in equatorial regions on Mars.

Another useful tool to test the depth of the suggested global hydrosphere/cryosphere on Mars (Clifford 1993) is the analysis of other large craters where the time of the impact is relatively known. A detailed study of the Amazonian-aged Lyot crater, 215 km in diameter and located at 50°N and 30°E, shows no evidence for hydrothermal activity or melting of ground ice as expected from the impact process (Russell and Head 2002). This result may indicate a local absence of groundwater and ground ice at the time of the impact (Russell and Head 2002), which would be in agreement with our results.

Although fluvial processes have been active and near-surface water and/or ice were likely existing in all regions, it is obvious that the onset diameter of rampart craters varies strongly. Unusually small rampart craters (~1 km) occur in the Hesperian units across Valles Marineris (Reiss et al. 2005). The onset diameter in the Xanthe Terra region is ~4 km and in southern Chryse Planitia is ~3 km. These differences may also be explained by decreasing erosion rates throughout Martian history as well as throughout the duration of fluvial processes. Small ramparts in the Xanthe Terra region that formed in the Noachian eroded subsequently due to high erosion rates in the Noachian (Carr 1992; Craddock and Maxwell 1993; Craddock et al. 1997; Hartmann et al. 1999). Small rampart craters formed in the Hesperian resisted the lower erosion rates at these times (Arvidson et al. 1979; Carr 1992; Golombek and Bridges 2000) and are still visible today. The lack of smaller rampart craters on Amazonian-aged units of southern Chryse Planitia could be due to short-lived catastrophic fluvial processes (e.g., Baker 1982), which did not last long enough for rampart crater formation by relatively rare impact events. This scenario would be consistent with the observation of small onset diameters (3 km) on Hesperian units in Solis Planum (Barlow et al. 2001).

There are many analyses supporting the role of subsurface volatiles causing the layered ejecta morphology around Martian craters, but some characteristics could also produced by atmospheric interactions (see review by Barlow 2005). The coincidence of the rampart crater ages with periods of fluvial activity indicates that liquid H_2O and/or subsurface ice were abundant at the time of the impacts. This may be another argument against an atmospheric-only origin of rampart craters, which does not exclude that atmospheric effects contributed in the formation of the layered ejecta blankets.

Our results question the method of determining the present-day equatorial ground-ice depths from the onset diameter of rampart craters. If most rampart craters are old, then the onset diameters only reflect the ground ice table depth at or shortly after their formation on ancient Mars.

Rampart craters may only reflect past ground-ice depths and are therefore relics of the possibly warmer and wetter climate on an ancient Mars. However, our study is regionally limited and younger and smaller equatorial rampart craters may occur on a global scale.

The current and upcoming radar experiments MARSIS and SHARAD of the Mars Express and Mars Reconnaissance Orbiter missions might be able to determine the present-day equatorial ground-ice depth. Initial MARSIS results may indicate a possible ice-rich low-mass deposit more than 1 km thick above the 2–2.5 km deep base of a buried quasi-circular structure in Chryse Planitia at 36°N and 337.5°E (Picardi et al. 2005), which has been interpreted as an impact basin about 250 km in diameter and is near our study region in southern Chryse Planitia at 20°N and 325.5°E. If this deposit is ice-rich, then it lies in a depth of more than ~1 km, which is much deeper than the expected roof of the ice-rich zone at 30° latitude in depths of 200 m to 250 m from the onset diameter of rampart craters (Squyres et al. 1992). This is in agreement with our results of a lowering of the ground-ice table with time. However, although the interpretation of the MARSIS data as an ice-rich deposit is uncertain and regionally limited, the first results are promising to constrain the depth of volatile-rich deposits with the radar experiments in the future.

CONCLUSIONS

1. The absolute model ages of rampart craters in three equatorial regions indicate that the formation is connected to volatile-rich periods in Martian history. The onset diameter indicates the shallowest ground ice table in Xanthe Terra at around 3.8 Gyr, in the Valles Marineris region at around 3.6 Gyr and in southern Chryse Planitia at around 1.5 Gyr. These ages are consistent with periods of fluvial activity in the study regions, which may be another argument against an atmospheric-only origin of rampart craters.
2. The lack of smaller Amazonian-aged rampart craters and the increase of onset diameter with time in the Xanthe Terra and Valles Marineris regions suggest that the present ground ice table could be more than one kilometer deep or non-existent. In southern Chryse Planitia, one small (3 km), relatively young (~1.5 Gyr) rampart crater indicates that ground ice was present at depths of ≤300 m. However, the loss of volatiles might have lowered the ground ice table over the last 1.5 Gyr even in this region. Our results indicate a lowering of the ground ice table throughout Martian history in these regions.
3. The derived ages of rampart craters in the Valles Marineris region favor a formation of dendritic valley networks near Echus Chasma in the Early Hesperian at around 3.6 Gyr. This is in agreement with studies of Harrison and Grimm (2005), but is in contrast to the results of Mangold et al. (2004) and Quantin et al. (2005) that fluvial surface run-off occurred within the Late Hesperian in the Valles Marineris region.
4. The results of this study question the method of deriving present equatorial ground ice depths from the rampart crater onset diameter. The derived equatorial ground ice depths (300–400 m) of Kuzmin et al. (1988) from rampart crater onset diameters did not take into account the time of the impact events and the possible loss of volatiles through diffusion and sublimation throughout Martian history.

Acknowledgments–We thank the HRSC Experiment Teams at DLR Berlin and Freie Universitaet Berlin as well as the Mars Express Project Teams at ESTEC and ESOC for their successful planning and acquisition of data as well as for making the processed data available to the HRSC Team. We acknowledge the effort of the HRSC Co-Investigator Team members and their associates who have contributed to this investigation in the preparatory phase and in scientific discussions within the Team. This work was supported by the Programme National de Planétologie and by the European Community's Improving Human Potential Program under contract RTN2-2001-00414, MAGE. We thank Daniel Berman and Jim Head for helpful reviews and Nadine Barlow for helpful comments that greatly improved the manuscript.

Editorial Handling—Dr. Nadine Barlow

REFERENCES

Allen C. C. 1979. Areal distribution of Martian rampart craters. *Icarus* 39:111–123.

Arvidson R., Guiness E., and Lee S. 1979. Differential aeolian redistribution rates on Mars. *Nature* 278:533–535.

Baker V. R. 1982. *The channels of Mars*. Austin, Texas: University of Texas Press. 198 p.

Baker V. R. and Kochel R. C. 1979. Martian channel morphology—Maja and Kasei Valles. *Journal of Geophysical Research* 84: 7961–7983.

Barlow N. G. 2004. Martian subsurface volatile concentrations as a function of time: Clues from layered ejecta craters. *Geophysical Research Letters* 31, doi:10.1029/2003GL019075.

Barlow N. G. 2005. A review of Martian impact crater ejecta structures and their implications for target properties. In *Large meteorite impacts III*, edited by Kenkmann T., Hörz F., and Deutsch A. Boulder, Colorado: Geological Society of America. pp. 433–442.

Barlow N. G. and Bradley T. L. 1990. Martian impact craters—Correlations of ejecta and interior morphologies with diameter, latitude, and terrain. *Icarus* 87:156–179.

Barlow N. G., Boyce J. M., Costard F. M., Craddock R. A., Garvin J. B., Sakimoto S. E. H., Kuzmin R. O., Roddy D. J., and Soderblom L. A. 2000. Standardizing the nomenclature of Martian impact crater ejecta morphologies. *Journal of Geophysical Research* 105:26,733–26,738.

Barlow N. G., Koroshetz J., and Dohm J. M. 2001. Variations in the

onset diameter for Martian layered ejecta morphologies and their implications for subsurface volatile reservoirs. *Geophysical Research Letters* 28:3095–3098.

Barnouin-Jha O. S. and Schultz P. H. 1998. Lobateness of impact ejecta deposits from atmospheric interactions. *Journal of Geophysical Research* 103:25,739–25,756.

Barnouin-Jha O. S., Schultz P. H., and Lever J. H. 1999a. Investigating the interactions between an atmosphere and an ejecta curtain, 1, Wind tunnel tests. *Journal of Geophysical Research* 104:27,105–27,116.

Barnouin-Jha O. S., Schultz P. H., and Lever J. H. 1999b. Investigating the interactions between an atmosphere and an ejecta curtain, 2, Numerical experiments. *Journal of Geophysical Research* 104:27,117–27,132.

Boyce J. M. and Witbeck N. E. 1980. Distribution of thermal gradient values in the equatorial region of Mars based on impact crater morphology. Reports of Planetary Geology Program. NASA Technical Memorandum 82385. pp. 140–143.

Carr M. H. 1992. Post-Noachian erosion rates: Implications for Mars climate change (abstract). 23rd Lunar and Planetary Science Conference. pp. 205–206.

Carr M. H. 1996. *Water on Mars*. New York: Oxford University Press. 229 p.

Carr M. H. and Clow G. D. 1981. Martian channels and valleys—Their characteristics, distribution, and age. *Icarus* 48:91–117.

Carr M. H., Crumpler L. S., Cutts J. A., Greeley R., Guest J. E., and Masursky H. 1977. Martian impact craters and emplacement of ejecta by surface flow. *Journal of Geophysical Research* 82: 4055–4065.

Carr M. H. and Malin M. C. 2000. Meter-scale characteristics of Martian channels and valleys. *Icarus* 146:366–386.

Clifford S. M. 1993. A model for the hydrologic and climatic behavior of water on Mars. *Journal of Geophysical Research* 98: 10,973–11,016.

Clifford S. M. and Hillel D. 1983. The stability of ground ice in the equatorial region of Mars. *Journal of Geophysical Research* 88: 2456–2474.

Costard F. M. 1989. The spatial distribution of volatiles in the Martian hydrolithosphere. *Earth, Moon, and Planets* 45:265–290.

Craddock R. A. and Maxwell T. A. 1993. Geomorphic evolution of the Martian highlands through ancient fluvial processes. *Journal of Geophysical Research* 98:3453–3468.

Craddock R. A., Maxwell T. A., and Howard A. D. 1997. Crater morphometry and modification in the Sinus Sabaeus and Margaritifer Sinus regions of Mars. *Journal of Geophysical Research* 102:13,321–13,340.

Croft S. K. 1985. The scaling of complex craters. *Journal of Geophysical Research* 90:828–842.

Crumpler L. S. 1997. Geotraverse from Xanthe Terra to Chryse Planitia: Viking 1 Lander region, Mars. *Journal of Geophysical Research* 102:4201–4218.

Di Achille G., Marinangeli L., Ori G. G., Hauber E., Gwinner K., Reiss D., and Neukum G. 2006. Geological evolution of the Tyras Vallis paleolacustrine system, Mars. *Journal of Geophysical Research* 111, doi:10.1029/2005JE002561.

Fanale F. P., Salvail J. R., Zent A. P., and Postawko S. E. 1986. Global distribution and migration of subsurface ice on Mars. *Icarus* 67: 1–18.

Garvin J. B., Sakimoto S. E. H., Frawley J. J., and Schnetzler C. 2000. North polar region craterforms on Mars: Geometric characteristics from the Mars Orbiter Laser Altimeter. *Icarus* 144:329–352.

Gendrin A., Mangold N., Bibring J.-P., Langevin Y., Gondet B., Poulet F., Bonello G., Quantin C., Mustard J., Arvidson R., and LeMouélic S. 2005. Sulfates in Martian layered terrains: The OMEGA/Mars Express View. *Science* 307:1587–1591.

Golombek M. P., Cook R. A., Moore H. J., and Parker T. J. 1997. Selection of the Mars Pathfinder landing site. *Journal of Geophysical Research* 102:3967–3988.

Golombek M. P. and Bridges N. T. 2000. Erosion rates on Mars and implications for climate change: Constraints from the Pathfinder landing site. *Journal of Geophysical Research* 105: 1841–1854.

Golombek M. P., Grant J. A., Crumpler L. S., Greeley R., Arvidson R. E., and the Athena Science Team. 2005. Climate change from the Mars Exploration Rover landing sites: From wet in the Noachian to dry and desiccating since the Hesperian (abstract #1539). 36th Lunar and Planetary Science Conference. CD-ROM.

Harrison K. P. and Grimm R. E. 2005. Groundwater-controlled valley networks and the decline of surface runoff on early Mars. *Journal of Geophysical Research* 110, doi:10.1029/2005JE002455.

Hartmann W. K. 1977. Relative crater production rates on planets. *Icarus* 31:260–276.

Hartmann W. K. 2005. Martian cratering 8: Isochron refinement and the chronology of Mars. *Icarus* 174:294–320.

Hartmann W. K. and Neukum G. 2001. Cratering chronology and the evolution of Mars. *Space Science Reviews* 96:165–194.

Hartmann W. K., Malin M., McEwen A., Carr M. H., Soderblom L., Thomas P., Danielson E., James P., and Veverka J. 1999. Evidence for recent volcanism on Mars from crater counts. *Nature* 397:586–589.

Hauber E., Gwinner K., Reiss D., Scholten F., Michael G. G., Jaumann R., Ori G. G., Marinangeli L., Neukum G., and the HRSC Co-Investigator Team. 2005. Delta-like deposits in Xanthe Terra, Mars, as seen with the High-Resolution Stereo Camera (HRSC) (abstract #1661). 36th Lunar and Planetary Science Conference. CD-ROM.

Head J. W. and Roth R. 1976. Mars pedestal crater escarpments: Evidence for ejecta-related emplacement (abstract). Symposium on Planetary Cratering Mechanics. pp. 50–52.

Higgins C. G. 1982. Drainage systems developed by sapping on Earth and Mars. *Geology* 10:147–152.

Ivanov B. A. 2001. Mars/Moon cratering rate ratio estimates. *Space Science Reviews* 96:87–104.

Ivanov M. A. and Head J. W. 2001. Chryse Planitia, Mars: Topographic configuration, outflow channel continuity and sequence, and tests for hypothesized ancient bodies of water using Mars Orbiter Laser Altimeter (MOLA) data. *Journal of Geophysical Research* 106:3275–3296.

Jernsletten J. A. 2004. A topographic test for the existence of ground ice in the walls of Coprates Chasma, Mars. *Journal of Geophysical Research* 109, doi:10.1029/2004JE002272.

Komatsu G. and Baker V. R. 1997. Paleohydrology and flood geomorphology of Ares Vallis. *Journal of Geophysical Research* 102:4151–4160.

Kuzmin R. O. 1980. Determination of frozen soil depth on Mars from the morphology of fresh craters. *Doklady Akademii Nauk SSR* 252:1445–1448.

Kuzmin R. O., Bobina N. N., Zabalueva E. V., and Shashkina V. P. 1988. Structural inhomogeneities of the Martian cryolithosphere. *Solar System Resarch* 22:121–133.

Kuzmin R. O., Bobina N. N., Zabalueva E. V., and Shashkina V. P. 1989. Structural irregularities of the upper layers of the Martian cryolithosphere. Proceedings, 28th International Geological Congress. pp. 80–95.

Lucchitta B. K. 1987. Valles Marineris, Mars—Wet debris flows and ground ice. *Icarus* 72:411–429.

Lucchitta B. K. 1998. Pathfinder landing site: Alternatives to

catastrophic floods and an Antarctic ice-flow analog for outflow channels on Mars (abstract #1287). 29th Lunar and Planetary Science Conference. CD-ROM.

Mangold N., Quantin C., Ansan V., Delacourt C., and Allemand P. 2004. Evidence for precipitation on Mars from dendritic valleys in the Valles Marineris area. *Science* 305:78–81.

Marchenko A. G., Basilevsky A. T., Hoffmann H., Hauber E., Cook A. C., and Neukum G. 1998. Geology of the common mouth of the Ares and Tiu Valles, Mars. *Solar System Research* 32:425–452.

Masursky H., Boyce J. M., Dial A. L., Schaber G. G., and Strobell M. E. 1977. Classification and time of formation of Martian channels based on Viking data. *Journal of Geophysical Research* 82:4016–4038.

Masursky H., Dial A. L., and Strobell M. E. 1980. Martian channels—A late Viking view. Reports of Planetary Geology Program. NASA Technical Memorandum 82385. pp. 184–187.

McEwen A. S., Preblich B. S., Turtle E. P., Artemieva N. A., Golombek M. P., Hurst M., Kirk R. L., Burr D. M., and Christensen P. R. 2005. The rayed crater Zunil and interpretations of small impact craters on Mars. *Icarus* 176:351–381.

Mellon M. T. and Jakosky B. M. 1995. The distribution and behavior of Martian ground ice during past and present epochs. *Journal of Geophysical Research* 100:11,781–11,800.

Mellon M. T., Jakosky B. M., and Postawko S. E. 1997. The persistence of equatorial ground ice on Mars. *Journal of Geophysical Research* 102:19,357–19,370.

Melosh H. J. 1989. *Impact cratering: A geologic process*. New York: Oxford University Press. 245 p.

Mouginis-Mark P. J. 1979. Martian fluidized crater morphology—Variations with crater size, latitude, altitude, and target material. *Journal of Geophysical Research* 84:8011–8022.

Mouginis-Mark P. J. 1987. Water or ice in the Martian regolith? Clues from rampart craters seen at very high resolution. *Icarus* 71:268–286.

Mouginis-Mark P. J., Boyce J. M., Hamilton V. E., and Anderson F. S. 2003. A very young, large, impact crater on Mars (abstract #3004). The Sixth International Conference on Mars. CD-ROM.

Nelson D. M. and Greeley R. 1999. Geology of Xanthe Terra outflow channels and the Mars Pathfinder landing site. *Journal of Geophysical Research* 104:8653–8670.

Neukum G. and Hiller K. 1981. Martian ages. *Journal of Geophysical Research* 86:3097–3121.

Neukum G. and Wise D. U. 1976. Mars—A standard crater curve and possible new time scale. *Science* 194:1381–1387.

Neukum G., Ivanov B. A., and Hartmann W. K. 2001. Cratering records in the inner solar system in relation to the lunar reference system. *Space Science Reviews* 96:55–86.

Neukum G., Jaumann R., Hoffmann H., Hauber E., Head J. W., Basilevsky A. T., Ivanov B. A., Werner S. C., van Gasselt S., Murray J. B., McCord T., and the HRSC Co-Investigator Team. 2004a. Recent and episodic volcanic and glacial activity on Mars revealed by the High-Resolution Stereo Camera. *Nature* 432: 971–979.

Neukum G., Jaumann R., and the HRSC Co-Investigator and Experiment Team. 2004b. HRSC: The High-Resolution Stereo Camera of Mars Express. In *Mars Express: The scientific payload*, edited by Wilson A. Noordwijk, The Netherlands: ESA Publications Division. pp. 17–35.

Peulvast J.-P., Mége D., Chiciak J., Costard F., and Masson P. 2001. Morphology, evolution and tectonics of Valles Marineris wallslopes (Mars). *Geomorphology* 37:329–352.

Picardi G., Plaut J. J., Biccari D., Bombaci O., Calabrese D., Cartacci M., Cicchetti A., Clifford S. M., Edenhofer P., Farrell W. M., Federico C., Frigeri A., Gurnett D. A., Hagfors T., Heggy E., Herique A., Huff R. L., Ivanov A. B., Johnson W. T. K., Jordan R. L., Kirchner D. L., Kofman W., Leuschen C. J., Nielsen E., Orosei R., Pettinelli E., Phillips R. J., Plettemeier D., Safaeinili A., Seu R., Stofan E. R., Vannaroni G., Watters T. R., and Zampolini E. 2005. Radar soundings of the subsurface of Mars. *Science* 310:1925–1928.

Quantin C., Allemand P., Mangold N., and Delacourt C. 2004. Ages of Valles Marineris (Mars) landslides and implications for canyon history. *Icarus* 172:555–572.

Quantin C., Allemand P., Mangold N., Dromart G., and Delacourt C. 2005. Fluvial and lacustrine activity on layered deposits in Melas Chasma, Valles Marineris, Mars. *Journal of Geophysical Research* 110, doi:10.1029/2005JE002440.

Reiss D., Hauber E., Michael G., Jaumann R., and Neukum G. 2005. Small rampart craters in an equatorial region on Mars: Implications for near-surface water or ice. *Geophysical Research Letters* 32, doi: 10.1029/2005GL022758.

Rotto S. and Tanaka K. L. 1995. Geologic map of Mars. USGS Miscellaneous Investigations Series Map I-2241. Scale 1: 15,000,000.

Russell P. S. and Head J. W. 2002. The Martian hydrosphere/cryosphere system: Implications of the absence of hydrologic activity at Lyot crater. *Geophysical Research Letters* 29, doi: 10.1029/2002GL015178.

Schultz P. H. 1992. Atmospheric effects on ejecta emplacement. *Journal of Geophysical Research* 97:11,623–11,662.

Schultz P. H. and Gault D. E. 1979. Atmospheric effects on Martian ejecta emplacement. *Journal of Geophysical Research* 84:7669–7687.

Scott D. H. and Tanaka K. L. 1986. Geologic map of the western equatorial region of Mars. USGS Miscellaneous Investigations Series Map I-1802-A. Scale 1:15,000,000.

Soderblom L. A., West R. A., Herman B. M., Kreidler T. J., and Condit C. D. 1974. Martian planetwide crater distributions: Implications for geologic history and surface processes. *Icarus* 22:239–263.

Squyres S. W., Clifford S. M., Kuzmin R. O., Zimbelman J. R., and Costard F. M. 1992. Ice in the Martian regolith. In *Mars*, edited by Kieffer H. H., Jakosky B. M., Synder C. W. and Matthews M. S. Tucson, Arizona: The University of Arizona Press. pp. 523–554.

Stöffler D. and Ryder G. 2001. Stratigraphy and isotope ages of lunar geologic units: Chronological standard for the inner solar system. *Space Science Reviews* 96:9–54.

Tanaka K. L. 1997. Sedimentary history and mass flow structures of Chryse and Acidalia Planitiae, Mars. *Journal of Geophysical Research* 102:4131–4150.

Tanaka K. L. 1999. Debris-flow origin for the Simud/Tiu deposit on Mars. *Journal of Geophysical Research* 104:8637–8652.

Werner S. C., Ivanov B. A., and Neukum G. 2006. Secondary cratering and age determination on Mars (abstract #1595). 37th Lunar and Planetary Science Conference. CD-ROM.

Wohletz K. H. and Sheridan M. F. 1983. Martian rampart crater ejecta—Experiments and analysis of melt-water interaction. *Icarus* 56:15–37.